SEARCH FOR PRODUCTION OF A HIGGS BOSON AND A SINGLE TOP QUARK IN MULTILEPTON FINAL STATES IN pp COLLISIONS AT $\sqrt{s} = 13$ TeV.

by

Jose Andres Monroy Montañez

A DISSERTATION

Presented to the Faculty of

The Graduate College at the University of Nebraska

In Partial Fulfilment of Requirements

For the Degree of Doctor of Philosophy

Major: Physics and Astronomy

Under the Supervision of Kenneth Bloom and Aaron Dominguez

Lincoln, Nebraska

July, 2018

SEARCH FOR PRODUCTION OF A HIGGS BOSON AND A SINGLE TOP QUARK IN MULTILEPTON FINAL STATES IN pp COLLISIONS AT $\sqrt{s} = 13$ TeV.

Jose Andres Monroy Montañez, Ph.D.

University of Nebraska, 2018

Adviser: Kenneth Bloom and Aaron Dominguez

Table of Contents

Table of Contents iii

List of Figures iv

List of Tables v

1 Event generation, simulation and reconstruction 1

1.1 Event generation 2

1.2 Monte Carlo Event Generators. 6

1.3 CMS detector simulation. 7

1.4 Event reconstruction. 9

1.4.1 Particle-Flow Algorithm. 10

1.4.2 Event reconstruction examples 21

Bibliography 22

References 24

List of Figures

1.1 Event generation process. 2
1.2 Jet reconstruction. 17
1.3 Jet energy corrections. 18
1.4 Secondary vertex in a b-hadron decay. 20
1.5 Recorded events reconstruction. 23

List of Tables

Chapter 1

Event generation, simulation and reconstruction

The process of analyzing the data recorded by the CMS experiment involves several stages where the data are processed in order to interpret the information provided by all the detection systems; in those stages, the particles produced after the *pp* collision are identified by reconstructing their trajectories and measuring their features. In addition, the SM provides a set of predictions that have to be compared with the experimental results; however, in most of the cases, theoretical predictions are not directly comparable to experimental results due to the diverse source of uncertainties introduced by the experimental setup and theoretical approximations, among others.

The strategy to face these conditions consists in using statistical methods implemented in computational algorithms to produce numerical results that can be contrasted with the experimental results. These computational algorithms are commonly known as Monte Carlo (MC) methods and, in the case of particle physics, they are designed to apply the SM rules and produce predictions about the physical observables measured in the experiments. Since particle physics is governed by quantum mechanics principles, predictions are not allowed for single events; therefore, a high number of events are "generated" and predictions are produced in the form of statistical distributions for the observables. Effects of the detector presence are included in the predictions by introducing simulations of the detector itself.

This chapter presents a description of the event generation strategy and the tools used to perform the detector simulation and physics objects reconstruction. A comprehensive review of event generators for LHC physics can be found in reference [79] on which this chapter is based.

1.1 Event generation

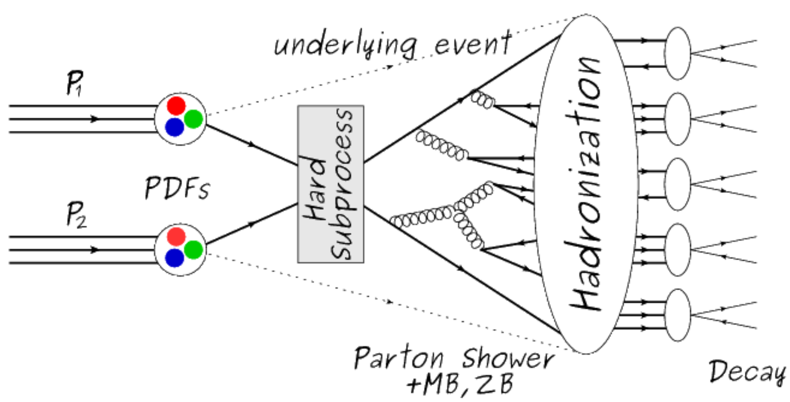

Figure 1.1: Event generation process. In the first step, the PDF of the colliding particles is considered so the specific interaction is described. The actual interaction is generated in the hard subprocess; the cross-section of the process is calculated from the matrix element connecting the initial and final states. The parton shower describes the evolution of the partons from the hard subprocess according to the DGLAP equations. At this step, the underlying event and PU effects are included in the generation. The resulting partons from the parton shower are recombined to form hadrons in the hadronization step; most of them are unstable, therefore, their decays are also generated in agreement to the known branching ratios. Modified from reference [80].

The event generation is intended to create events that mimic the behavior of actual events produced in pp collisions; they obey a sequence of steps from the particles collision hard process to the decay process into the final state particles. Figure 1.1 shows a schematic view of the event generation process; the fact that the full process can be treated as several independent steps is based on the QCD factorization theorem.

Generation starts by taking into account the PDFs of the incoming particles. Event generators offer the option to chose from several PDF sets depending on the particular process under simulation[1]; in the following pp collisions will be considered. The *hard subprocess* describes the actual interaction between partons from the incoming protons; it is represented by the matrix element connecting the initial and final states of the interaction. Normally, the matrix element can be written as a sum over Feynman diagrams and consider interferences between terms in the summation. During the generation of the hard subprocess, the production cross section is calculated.

The order to which the cross section is calculated depends on the order of the Feynman diagrams involved in the calculation; therefore, radiative corrections are included by considering a higher order Feynman diagrams where QCD radiation dominates. Currently, cross sections calculated to LO do not offer a satisfactory description of the processes, i.e., the results are only reliable for the shape of distributions; therefore, NLO calculations have to be performed with the implication that the computing time needed is highly increased.

The final parton content of the hard subprocess is subjected to the *parton shower* which generates the gluon radiation. Parton shower evolves the partons; i.e., glouns

[1] Tool in Reference [81] allows to plot different PDF sets under customizable conditions.

split into quark-antiquark pairs and quarks of enough energy radiate gluons giving rise to further parton multiplication, following the DGLAP (Dokshitzer-Gribov-Lipatov-Altarelli-Parisi) equations. Showering continues until the energy scale is low enough to reach the non-perturbative limit.

In the simulation of LHC processes that involve b quarks, like the single top quark or Higgs associated production, it is needed to consider that the b quark is heavier than the proton; in this sense, the QCD interaction description is made in two different schemes [82]

- four-flavor (4F) scheme. b quarks appear only in the final state because they are heavier than the proton and therefore they can be produced only from the splitting of a gluon into pairs or singly in association with a t quark in high energy-scale interactions. During the simulation, the b-PDFs are set to zero because they cannot be part of the proton. Calculations in this scheme are more complicated due to the presence of the second b quark but the full kinematics is considered already at LO and therefore the accuracy of the description is better.

- five-flavor (5F) scheme. b quarks are considered massless, therefore they can appear in both initial and final states since they can now be part of the proton; thus, during the simulation b-PDFs are not set to zero. In this scheme, calculations are simpler than in the 4F scheme and possible logarithmic divergences are absorbed by the PDFs through the DGLAP evolution.

In this thesis, the tHq events are generated using the 4F scheme in order to reduce uncertainties, while the tHW events are generated using the 5F scheme to eliminate LO interference with the $t\bar{t}H$ process [48].

Partons involved in the *pp* collision are the focus of the simulation, however, the rest of the partons inside the incoming protons are also affected because the remnants are colored objects; also, multiple parton interactions can occur. The hadronization of the remnants and multiple parton interactions are known as “underlying event” and it has to be included in the simulation. In addition, multiple *pp* collisions in the same bunch crossing (pile-up mentioned in **??**) occurs, actually in two forms

- *in-time PU* which refers to multiple *pp* collision in the bunch crossing but that are not considered as primary vertices.
- *Out-of-time PU* which refers to overlapping *pp* collisions from consecutive bunch crossings; this can occur due to the time-delays in the detection systems where information from one bunch crossing is assigned to the next or previous one.

While the underlying event effects are included in generation using generator-specific tools, PU effects are added to the generation by overlying Minimum-bias (MB) and Zero-bias (ZB) events to the generated events. MB events are inelastic events selected by using a loose (minimum bias) trigger with as little bias as possible, therefore accepting a large fraction of the overall inelastic event; ZB events correspond to random events recorded by the detector when collisions are likely. MB models in-time PU and ZB models out-of-time PU.

The next step in the generation process is called “hadronization”. Since particles with a net color charge are not allowed to exits isolated, they have to recombine to form bound states. This is precisely the process by which the partons resulting from the parton shower arrange themselves as color singlets to form hadrons. At this step, the energy-scale is low and the strong coupling constant is large, therefore hadronization process is non-perturbative and the evolution of the partons is described using phenomenological models. Most of the baryons and mesons produced in the hadronization are unstable and hence they will decay in the detector.

The last step in the generation process corresponds to the decay of the unstable particles generated during hadronization; it is also simulated in the hadronization step, based on the known branching ratios.

1.2 Monte Carlo Event Generators.

The event generation described in the previous section has been implemented in several software packages for which a brief description is given.

- **PYTHIA 8**. It is a program designed to perform the generation of high energy physics events which describe the collisions between particles such as electrons, protons. Several theories and models are implemented in it, in order to describe physical aspects like hard and soft interaction, parton distributions, initial and final-state parton showers, multiple parton interactions, beam remnants, hadronization[2] and particle decay. Thanks to extensive testing, several optimized parametrizations, known as "tunings", have been defined in order to improve the description of actual collisions to a high degree of precision; for analysis at $\sqrt{s} = 13$ TeV, the underline event CUETP8M1 tune is employed [84]. The calculation of the matrix element is performed at LO which is not enough for the current required level of precision; therefore, pythia is often used for parton shower, hadronization and decays, while other event generators are used to generate the matrix element at NLO.

[2] based in the Lund string model [83]

- **MadGraph5_aMC@NLO**. MadGraph is a matrix element generator which calculates the amplitudes for all contributing Feynman diagrams of a given process but does not provide a parton shower while MC@NLO incorporate NLO QCD matrix elements consistently into a parton shower framework; thus, MadGraph5_aMC@NLO, as a merger of the two event generators MadGraph5 and aMC@NLO, is an event generator capable to calculate tree-level and NLO cross sections and perform the matching of those with the parton shower. It is one of the most frequently used matrix element generators; however, it has the particular feature of the presence of negative event weights which reduce the number of events used to reproduce the properties of the objects generated [85].

- **POWHEG**. It is an NLO matrix element generator where the hardest emission of color charged particles is generated in such a way that the negative event weights issue of MadGraph5_aMC@NLO is overcome; however, the method requires an interface with p_T-ordered parton shower or a parton shower generator where this highest emission can be vetoed in order to avoid double counting of this highest-energetic emission. PYTHIA is a commonly matched to POWHEG event generator [86].

Events resulting from the whole generation process are known as MC events.

1.3 CMS detector simulation.

After generation, MC events contain the physics of the collisions but they are not ready to be compared to the events recorded by the experiment since these recorded events correspond to the response of the detection systems to the interaction with the particles traversing them. The simulation of the CMS detector has to be applied on top of the event generation; it is simulated with a MC toolkit for the simulation of particles passing through matter called Geant4 which is also able to simulate the electronic signals that would be measured by all detectors inside CMS.

The simulation takes the generated particles contained in the MC events as input, makes them pass through the simulated geometry, and models physics processes that particles experience during their passage through matter. The full set of results from particle-matter interactions correspond to the simulated hit which contains information about the energy loss, momentum, position. Particles of the input event are called "primary", while the particles originating from GEANT4-modeled interactions of a primary particle with matter are called a "secondary". Simulated hits are the input of subsequent modules that emulate the response of the detector readout system and triggers. The output from the emulated detection systems and triggers is known as digitization [87, 88].

The modeling of the CMS detector corresponds to the accurate modeling of the interaction among particles, the detector material, and the magnetic field. This simulation procedure includes the following standard steps

- Modeling of the Interaction Region.
- Modeling of the particle passage through the hierarchy of volumes that compose CMS detector and of the accompanying physics processes.
- Modeling of the effect of multiple interactions per beam crossing and/or the effect of events overlay (Pile-Up simulation).

- Modeling of the detector's electronics response, signal shape, noise, calibration constants (digitization).

In addition to the full simulation, i.e. a detailed detector simulation, a faster simulation (FastSim) have been developed, that may be used where much larger statistics are required. In FastSim, detector material effects are parametrized and included in the hits; those hits are used as input of the same higher-level algorithms[3] used to analyze the recorded events. In this way, comparisons between fast and full simulations can be performed [90].

After the full detector simulation, the output events can be directly compared with events actually recorded in the CMS detector. The collection of MC events that reproduce the expected physics for a given process are known as MC samples.

1.4 Event reconstruction.

In contrast to MC samples for which all the particles' information is available from it's identity to its mass and energy, recorded events contain the electronic signals, provided by the CMS detection systems, encoding the interaction of physical particles with the detector matter; these electronic signals have to be combined in order to identify these particles and measure their features, i.e., particles have to be "reconstructed" using the signals provided by the detection systems. The CMS experiment use the "particle-flow event reconstruction algorithm (PF)" to do the reconstruction of particles produced in pp collisions. Next sections will present a basic description

[3] track fitting, calorimeter clustering, b tagging, electron identification, jet reconstruction and calibration, trigger algorithms which will be considered in the next sections

of the *Elements* used by PF (tracker tracks, energy clusters, and muon tracks), based in the references [91, 92] where more detailed descriptions can be found.

1.4.1 Particle-Flow Algorithm.

Each of the several sub detection systems of the CMS detector is dedicated to identifying a specific type of particles, i.e., photons and electrons are absorbed by the ECAL and their reconstruction is based on ECAL information; hadrons are reconstructed from clusters in the HCAL while muons are reconstructed from hits in the muon chambers. PF is designed to correlate signals from all the detector layers (tracks and energy clusters) in order to reconstruct and identify each final state particle and its properties. For instance, a charged hadron is identified by a geometrical connection, known as *link* between one or more calorimeter clusters and a track in the tracker provided there are no hits in the muon system; combining several measurements allows a better determination of the energy and charge sign of the charged hadron.

Charged-particle track reconstruction.

The strategy used by PF in order to reconstruct tracks is called "Iterative Tracking" which occurs in four steps

- Seed generation where initial track candidates are found by looking for a combination of hits in the pixel detector, strip tracker, and muon chambers. In total ten iterations are performed, each one with a different seeding requirement. Seeds are used to estimate the trajectory parameters and uncertainties at the time of the full track reconstruction. Seeds are also considered track candidates.
- Track finding using a tracking software known as Combinatorial Track Finder (CTF) [93]. The seed trajectories are extrapolated along the expected flight

path of a charged particle, in agreement to the trajectory parameters obtained in the first step, in an attempt to find additional hits that can be assigned to the track candidates.

- Track-fitting where the found tracks are passed as input to a module which provides the best estimate of the parameters of each trajectory.
- Track selection where track candidates are submitted to a selection which discards those that fail a set of defined quality criteria.

Iterations differ in the seeding configuration and the final track selection as elaborated in references [91, 92]. In the first iteration, high p_T tracks and tracks produced near to the interaction region are identified and those hits are masked thereby reducing the combinatorial complexity. Next iterations search for more complicated tracks, like low p_T tracks and tracks from b hadron decays, which tend to be displaced from the interaction region.

Vertex reconstruction.

During the track reconstruction, an extrapolation toward to the calorimeters is performed in order to match energy deposits; that extrapolation is performed also toward the beamline in order to find the origin of the track known as *vertex*. The vertex reconstruction is performed by selecting from the available reconstructed tracks, those that are consistent with being originated in the interaction region where *pp* collisions are produced. The selection involves a requirement on the number of tracker (pixel and strip) hits and the goodness of the track fit.

Selected tracks are clustered using a “deterministic annealing algorithm (DA)”[4]. A set of candidate vertices and their associated tracks, resulting from the DA, are then fitted with an “adaptive vertex fitter (AVF)” to produce the best estimate of the vertices locations.

The p_T of the several tracks associated to a reconstructed vertex is added, squared and used to organize the vertices; the vertex with the highest squared sum is designated as the *primary vertex (PV)* while the rest are designated as PU vertices.

Calorimeter clustering.

After traversing the CMS tracker system, electrons, photons and hadrons deposit their energy in the ECAL and HCAL cells. The PF clustering algorithm aims to provide a high detection efficiency even for low-energy particles and an efficient distinction between close energy deposits. The clustering runs independently in the ECAL barrel and endcaps, HCAL barrel and endcaps, and the two preshower layers, following two steps

- cells with an energy larger than a given seed threshold and larger than the energy of the neighboring cells are identified as cluster seeds. The neighbor cells are those that either share a side with the cluster seed candidate, or the eight closest cells including cells that only share a corner with the seed candidate.
- cells with at least a corner in common with a cell already in the cluster seed and with an energy above a cell threshold are grouped into topological clusters.

Clusters formed in this way are known as *particle-flow clusters*. With this clustering strategy, it is possible to detect and measure the energy and direction of photons and

[4] DA algorithm and AVF are described in detail in references [95, 96]

neutral hadrons as well as differentiate these neutral particles from the charged hadron energy deposits. In cases involving charged hadrons for which the track parameters are not determined accurately, for instance, low-quality and high-p_T tracks, clustering helps in the energy measurements.

Electron track reconstruction.

Although the charged-particle track reconstruction described above works for electrons, they lose a significant fraction of their energy via bremsstrahlung photon radiation before reaching the ECAL; thus, the reconstruction performance depends on the ability to measure also the radiated energy. The reconstruction strategy, in this case, requires information from the tracking system and from the ECAL. Bremsstrahlung photons are emitted at similar η values to that of the electron but at different values of ϕ; therefore, the radiated energy can be recovered by grouping ECAL clusters in a η window over a range of ϕ around the electron direction. The group is called ECAL supercluster.

Electron candidates from the track-seeding and ECAL super clustering are merged into a single collection which is submitted to a full electron tracking fit with a Gaussian-sum filter (GSF) [94]. The electron track and its associated ECAL supercluster form a *particle-flow electron*.

Muon track reconstruction.

Given that the CMS detector is equipped with a muon spectrometer capable to identify and measure the momentum of the muons traversing it, the muon reconstruction is not specific to PF; therefore, three different muon types are defined

- *Standalone muon.* A clustering on the DTs or CSCs hits is performed to form track segments; those segments are used as seeds for the reconstruction in the muon spectrometer. All DTs, CSCs, and RPCs hits along the muon trajectory are combined and fitted to form the full track. The fitting output is called a *standalone-muon track*.

- *tracker muon.* Each track in the inner tracker with p_T larger than 0.5 GeV and a total momentum p larger than 2.5 GeV is extrapolated to the muon system. A *tracker muon track* corresponds to the extrapolated tracks that match at least one muon segment.

- *Global muon.* When tracks in the inner tracker (inner tracks) and standalone-muon tracks are matched and turn out being compatibles, their hits are combined and fitted to form a *global-muon track*.

Global muons sharing the same inner track with tracker muons are merged into a single candidate. PF muon identification uses the muon energy deposits in ECAL, HCAL, and HO associated with the muon track to improve the muon identification.

Particle identification and reconstruction.

PF elements are connected by a linker algorithm that tests the connection between any pair of elements; if they are found to be linked, a geometrical distance that quantifies the quality of the link is assigned. Two elements may be linked indirectly through common elements. Linked elements form *PF blocks* and a PF block may contain elements originating in one or more particles. Links can be established between tracks, between calorimeter clusters, and between tracks and calorimeter clusters. The identification and reconstruction start with a PF block and proceeds as follows

- Muons. An "isolated global muon" is identified by evaluating the presence of inner track and energy deposits close to the global muon track in the (η,ϕ) plane, i.e., in a particular point of the global muon track, inner tracks and energy deposits are sought within a radius of $\Delta R = 0.3$ (see eqn. **??**) from the muon track; if they exit and the p_T of the found track added to the E_T of the found energy deposit does not exceed 10% of the muon p_T then the global muon is an isolated global muon. This isolation condition is stringent enough to reject hadrons misidentified as muons.

  "Non-isolated global muons" are identified using additional selection requirements on the number of track segments in the muon system and energy deposits along the muon track. Muons inside jets are identified with more stringent criteria in isolation and momentum as described in reference [97]. The PF elements associated with an identified muon are masked from the PF block.

- Electrons are identified and reconstructed as described above plus some additional requirements on fourteen variables like the amount of energy radiated, the distance between the extrapolated track position at the ECAL and the position of the associated ECAL supercluster, among others, which are combined in a specialized multivariate analysis strategy that improves the electron identification. Tracks and clusters used to identify and reconstruct electrons are masked in the PF block.

- Isolated photons are identified from ECAL superclusters with E_T larger than 10 GeV, for which the energy deposited at a distance of 0.15, from the supercluster position on the (η,ϕ) plane, does not exceed 10% of the supercluster energy; note that this is an isolation requirement. In addition, there must not be links to tracks. Clusters involved in the identification and reconstruction are masked in the PF block.

- Bremsstrahlung photons and prompt photons tend to convert to electron-positron pairs inside the tracker, therefore, a dedicated finder algorithm is used to link tracks that seem to originate from a photon conversion; in case those two tracks are compatible with the direction of a bremsstrahlung photon, they are also linked to the original electron track. Photon conversion tracks are also masked in the PF block.

- The remaining elements in the PF block are used to identify hadrons. In the region $|\eta| \leq 2.5$, neutral hadrons are identified with HCAL clusters not linked to any track while photons from neutral pion decays are identified with ECAL clusters without links to tracks. In the region $|\eta| > 2.5$ ECAL clusters linked to HCAL clusters are identified with a charged or neutral hadron shower; ECAL clusters with no links are identified with photons. HCAL clusters not used yet, are linked to one or more unlinked tracks and to an unlinked ECAL in order to reconstruct charged-hadrons or a combination of photons and neutral hadrons according to certain conditions on the calibrated calorimetric energy.

- Charged-particle tracks may be liked together when they converge to a "secondary vertex (SV) " displaced from the interaction point where the PV and PU vertices are reconstructed; at least three tracks are needed in that case, of which at most one has to be an incoming track with hits in tracker region between a PV and the SV.

The linker algorithm, as well as the whole PF algorithm, has been validated and commissioned; results from that validation are presented in the references [91].

Jet reconstruction.

Quarks and gluons may be produced in the *pp* collisions, therefore, their hadronization will be seen in the detector as a shower of hadrons and their decay products in the form of a "jet". The anti-k_t algorithm [98] is used to perform the jet reconstruction by clustering those PF particles within a cone (see figure 1.2); previously, isolated electrons, isolated muons, and charged particles associated with other interaction vertices are excluded from the clustering.

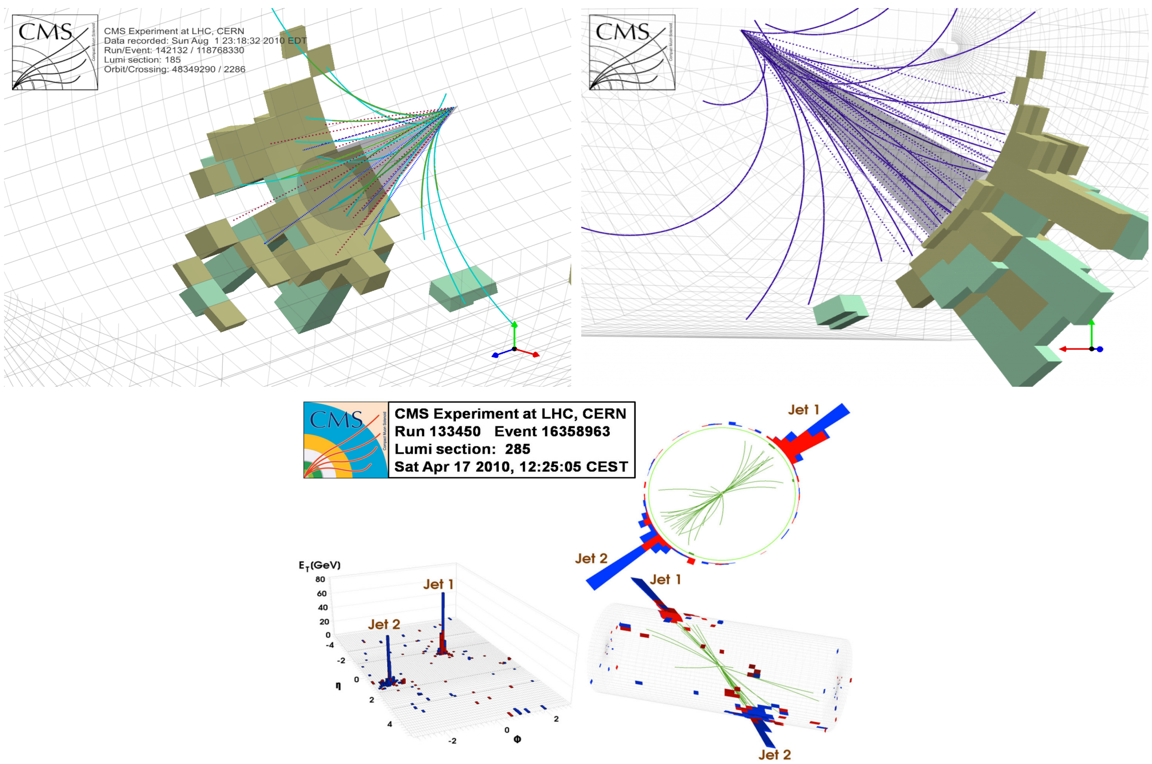

Figure 1.2: Jet reconstruction performed by the anti-k_t algorithm. Top: Two different views of a CMS recorded event are presented. Continuous lines correspond to the tracks left by charged particles in the tracker while dotted lines are the imaginary paths followed by neutral particles. The green cubes represent the ECAL cells while the blue ones represent the HCAL cells; in both cases, the height of the cube represent the amount of energy deposited in the cells [99]. Bottom: Reconstruction of a recorded event with two jets [100].

The anti-k_t algorithm proceeds in a sequential recombination of PF particles; the distance between particles i and j (d_{ij}) and the distance between particles and the beam are defined as

$$
\begin{aligned}
d_{ij} =& \min\left(\frac{1}{k_{ti}^2}, \frac{1}{k_{tj}^2}\right)\frac{\Delta_{ij}^2}{R^2} \\
d_{iB} =& \frac{1}{k_{ti}^2}
\end{aligned}
\tag{1.1}
$$

where $\Delta_{ij}^2 = (y_i - y_j)^2 + (\phi_i - \phi_j)^2$, k_{ti}, y_i and ϕ_i are the transverse momentum, rapidity and azimuth of particle i respectively and R is the called jet radius. For all the remaining PF particles, after removing the isolated ones, d_{ij} and d_{iB} are calculated[5] and the smallest is identified; if it is a d_{ij}, particles i and j are replaced with a new object whose momentum he vectorial sum of the combined particles. If the smallest distance is a d_{iB} the clustering process ends, the object i (which at this stage should be a combination of several PF particles) is declared as a *Particle-flow-jet* (PF jet) and all the associated PF particles are removed from the detector. The clustering process is repeated until no PF particles remain.

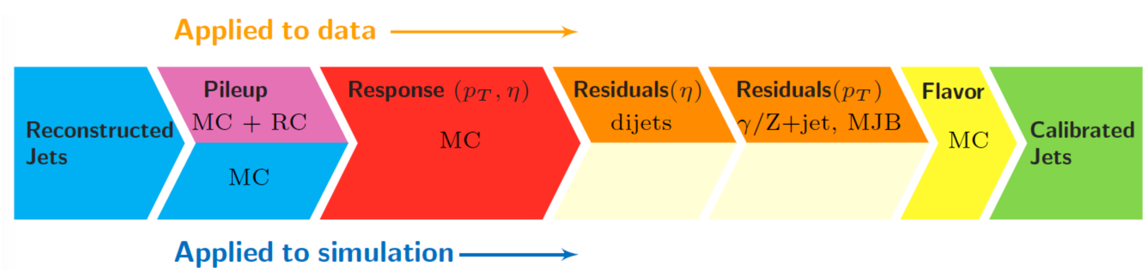

Figure 1.3: Jet energy correction diagram. Correction levels are applied sequentially in the indicated fixed order [102].

Even though jets can be reconstructed efficiently, there are some effects that are not included in the reconstruction and that lead to discrepancies between the reconstructed results and the predicted results; in order to overcome these discrepancies, a factor-

[5] Notice that this is a combinatorial calculation.

ized model has been designed in the form of jet energy corrections (JEC) [101, 102] applied sequentially as shown in the diagram of figure1.3.

At each level, the jet four-momentum is multiplied by a scaling factor based on jet properties, i.e., η, flavor, etc.

- Level 1 correction removes the energy coming from pile-up. The scale factor is determined using a MC sample of QCD dijet events with and without pileup overlay; it is parametrized in terms of the offset energy density ρ, jet area A, jet η and jet p_T. Different corrections are applied to data and MC due to the detector simulation.

- MC-truth correction accounts for differences between the reconstructed jet energy and the MC particle-level energy. The correction is determined on a QCD dijet MC sample and is parametrized in terms of the jet p_T and η.

- Residuals correct remaining small differences within jet response in data and MC. The Residuals η-dependent correction compares jets of similar p_T in the barrel reference region. The Residuals p_T-dependent correct the jet absolute scale (JES vs p_T).

- Jet-flavor corrections are derived in the same way as MC-truth corrections but using QCD pure flavor samples.

b-tagging of jets.

A particular feature of the hadrons containing bottom quarks (b-hadrons) is that they have a lifetime long enough to travel some distance before decaying, but it is not as long as those of light quark hadrons; therefore, when looking at the hadrons produced in pp collisions, b-hadrons decay typically inside the tracker rather than reach the calorimeters as some light-hadrons do. As a result, a b-hadron decay gives rise to a displaced vertex (secondary vertex) with respect to the primary vertex as shown in figure 1.4; the SV displacement is in the order of a few millimeters. A jet resulting from the decay of a b-hadron is called b jet; other jets are called light jets.

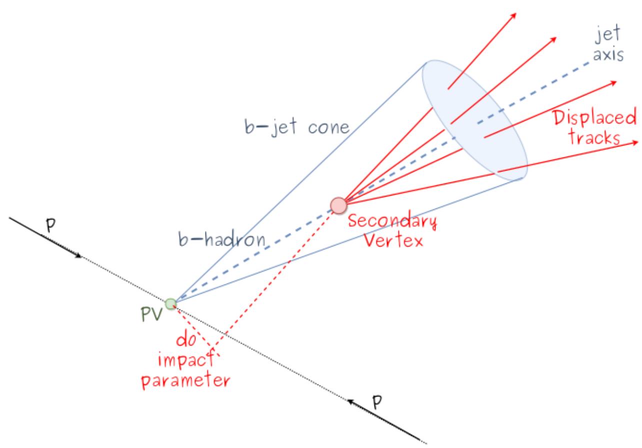

Figure 1.4: Secondary vertex in a b-hadron decay.

Several methods to identify b-jets (b-tagging) have been developed; the method used in this thesis is known as “Combined Secondary Vertex” algorithm in its second version (CSVv2) [103]. By using information of the impact parameter, the reconstructed secondary vertices and the jet kinematics in a multivariate analysis that combines the discrimination power of each variable in one global discriminator variable, three working points (references): loose, medium and tight, are defined which quantify the probabilities of mistag jets from light quarks as jets from b quarks; 10, 1 and 0.1 % respectively. Although the mistagging probability decrease with the working point strength, the efficiency to correctly tag b-jets also decrease as 83, 69 and 49 % for the respective working point; therefore, a balance needs to be achieved according to the specific requirements of the analysis.

Missing transverse energy.

The fact that proton bunches carry momentum along the z axis implies that for each event momentum balance in the transverse plane is expected. Imbalances are quantified by the missing transverse energy (MET) and are attributed to several sources including particles escaping undetected through the beam pipe, neutrinos produced in weak interactions processes which do not interact with the detector and thus escaping without leaving a sign, or even undiscovered particles predicted by models beyond the SM.

The PF algorithm assigns the negative sum of the momenta of all reconstructed PF particles to the *particle-flow MET* according to

$$\vec{\not{E}}_T = -\sum_i \vec{p}_{T,i} \tag{1.2}$$

JEC are propagated to the calculation of the $\vec{\not{E}}_T$ as described in the reference [104].

1.4.2 Event reconstruction examples

Figure 1.5 shows the results of the reconstruction performed on 3 recorded events. Descriptions are taken directly from the source.

- Top: “HIG-13-004 Event 1: Event recorded with the CMS detector in 2012 at a proton-proton center-of-mass energy of 8 TeV. The event shows characteristics expected from the decay of the SM Higgs boson to a pair of τ leptons. Such an event is characterized by the production of two forward-going jets, seen here in opposite endcaps. One of the τ decays to a muon (red lines on the right) and neutrinos, while the other τ decays into a charged hadron and a neutrino." [105].

- Center: "An $e\mu$ event candidate selected in 8 TeV data, as seen from the direction of the proton beams. The kinematics of the main objects used in the event selection are highlighted: two isolated leptons and two particle-flow jets. The reconstructed missing transverse energy is also displayed for reference" [106].

- Bottom: "Recorded event (ρ-z projection) with three jets with $p_T > 30$ GeV with one displaced muon track in 2016 data collected at 13 TeV. Each of the three jets has a displaced reconstructed vertex. The jet with $p_T(j) = 43.8$ GeV, $\eta(j) = -1.34$, $\phi(j) = -0.79$ contains muon with $p_T(\mu) = 5.5$ GeV, $\eta(\mu) = -1.25$, $\phi(\mu) = -0.84$. Event contains reconstructed isolated muon with $p_T(\mu) = 41.2$ GeV, $\eta(\mu) = 0.34$, $\phi(\mu) = 2.05$ and MET with $p_T = 72.5$ GeV, $\phi = -0.32$. Jet candidates for a b-jet from top quark leptonic and hadronic decays are tagged by CSVv2T algorithm. One of the other two jets is tagged by CharmT algorithm. Tracks with $p_T > 0.5$ GeV are shown. The number of reconstructed primary vertices is 18. Reconstructed m_T(W) is 101.8 GeV. Beam spot position correction is applied. Reconstructed primary vertices are shown in yellow color, while reconstructed displaced vertices and associated tracks are presented in black color. Dimensions are given in cm" [107].

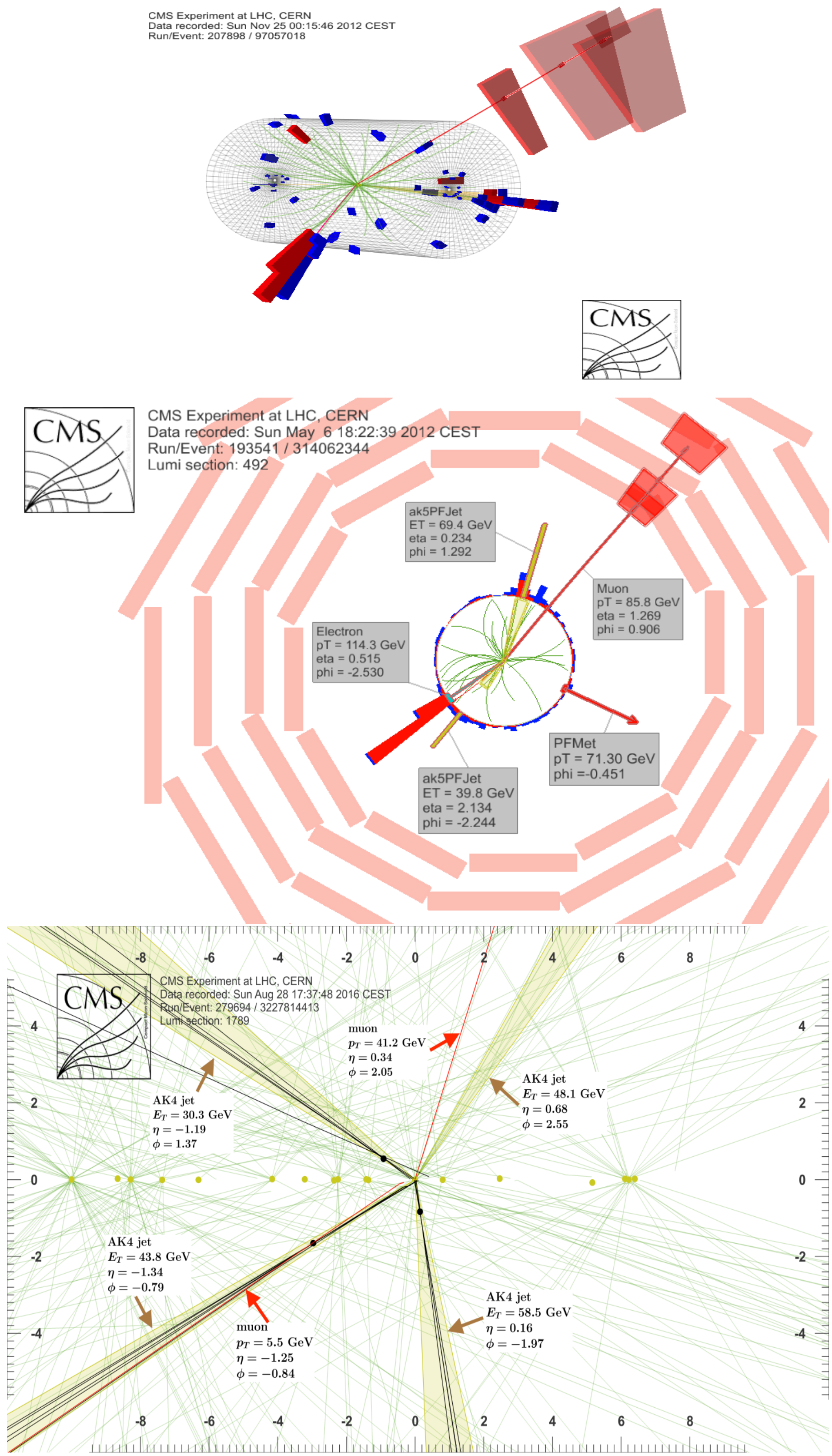

Figure 1.5: Recorded events reconstruction results; detailed description in text.

References

[1] J. Schwinger. “Quantum Electrodynamics. I. A Covariant Formulation”. Physical Review. 74 (10): 1439-61, (1948).

[2] R. P. Feynman. “Space-Time Approach to Quantum Electrodynamics”. Physical Review. 76 (6): 769-89, (1949).

[3] S. Tomonaga. “On a Relativistically Invariant Formulation of the Quantum Theory of Wave Fields”. Progress of Theoretical Physics. 1 (2): 27-42, (1946).

[4] D.J. Griffiths, “Introduction to electrodynamics”. 4th ed. Pearson, (2013).

[5] F. Mandl, G. Shaw. “Quantum field theory.” Chichester: Wiley (2009).

[6] F. Halzen, and A.D. Martin, “Quarks and leptons: An introductory course in modern particle physics”. New York: Wiley, (1984) .

[7] File: Standard_Model_of_Elementary_Particle_dark.svg. (2017, June 12) Wikimedia Commons, the free media repository. Retrieved November 27, 2017 from https://www.collegiate-advanced-electricity.com/single-post/2017/04/10/The-Standard-Model-of-Particle-Physics.

[8] E. Noether, “Invariante Variationsprobleme”, Nachrichten von der Gesellschaft der Wissenschaften zu Göttingen, mathematisch-physikalische Klasse, vol. 1918, pp. 235-257, (1918).

[9] C. Patrignani et al. (Particle Data Group), Chin. Phys. C, 40, 100001 (2016) and 2017 update.

[10] M. Goldhaber, L. Grodzins, A.W. Sunyar “Helicity of Neutrinos”, Phys. Rev. 109, 1015 (1958).

[11] Palanque-Delabrouille N et al. “Neutrino masses and cosmology with Lyman-alpha forest power spectrum”, JCAP 11 011 (2015).

[12] M. Gell-Mann. “A Schematic Model of Baryons and Mesons”. Physics Letters. 8 (3): 214-215 (1964).

[13] G. Zweig. “An SU(3) Model for Strong Interaction Symmetry and its Breaking” (PDF). CERN Report No.8182/TH.401 (1964).

[14] G. Zweig. “An SU(3) Model for Strong Interaction Symmetry and its Breaking: II” (PDF). CERN Report No.8419/TH.412(1964).

[15] M. Gell-Mann. “The Interpretation of the New Particles as Displaced Charged Multiplets”. Il Nuovo Cimento 4: 848. (1956).

[16] T. Nakano, K, Nishijima. “Charge Independence for V-particles”. Progress of Theoretical Physics 10 (5): 581-582. (1953).

[17] N. Cabibbo, “Unitary symmetry and leptonic decays” Physical Review Letters, vol. 10, no. 12, p. 531, (1963).

[18] M.Kobayashi, T.Maskawa, “CP-violation in the renormalizable theory of weak interaction,” Progress of Theoretical Physics, vol. 49, no. 2, pp. 652-657, (1973).

[19] File: Weak Decay (flipped).svg. (2017, June 12). Wikimedia Commons, the free media repository. Retrieved November 27, 2017 from

https://commons.wikimedia.org/w/index.php?title=File:Weak_Decay_(flipped).svg&oldid=247498592.

[20] Georgia Tech University. Coupling Constants for the Fundamental Forces(2005). Retrieved January 10, 2018, from http://hyperphysics.phy-astr.gsu.edu/hbase/Forces/couple.html#c2

[21] M. Strassler. (May 31, 2013).The Strengths of the Known Forces. Retrieved January 10, 2018, from https://profmattstrassler.com/articles-and-posts/particle-physics-basics/the-known-forces-of-nature/the-strength-of-the-known-forces/

[22] S.L. Glashow. “Partial symmetries of weak interactions”, Nucl. Phys. 22 579-588, (1961).

[23] A. Salam, J.C. Ward. “Electromagnetic and weak interactions”, Physics Letters 13 168-171, (1964).

[24] S. Weinberg, “A model of leptons”, Physical Review Letters, vol. 19, no. 21, p. 1264, (1967).

[25] M. Peskin, D. Schroeder, “An introduction to quantum field theory”. Perseus Books Publishing L.L.C., (1995).

[26] A. Pich. “The Standard Model of Electroweak Interactions” https://arxiv.org/abs/1201.0537

[27] F.Bellaiche. (2012, 2 September). “What’s this Higgs boson anyway?”. Retrieved from: https://www.quantum-bits.org/?p=233

[28] M. Endres et al. Nature 487, 454-458 (2012) doi:10.1038/nature11255

[29] F. Englert, R. Brout. “Broken Symmetry and the Mass of Gauge Vector Mesons”. Physical Review Letters. 13 (9): 321-23.(1964) doi:10.1103/PhysRevLett.13.321

[30] P.Higgs. “Broken Symmetries and the Masses of Gauge Bosons”. Physical Review Letters. 13 (16): 508-509,(1964). doi:10.1103/PhysRevLett.13.508.

[31] G.Guralnik, C.R. Hagen and T.W.B. Kibble. “Global Conservation Laws and Massless Particles”. Physical Review Letters. 13 (20): 585-587, (1964). doi:10.1103/PhysRevLett.13.585.

[32] CMS collaboration. “Observation of a new boson at a mass of 125 GeV with the CMS experiment at the LHC”. Physics Letters B. 716 (1): 30-61 (2012). arXiv:1207.7235. doi:10.1016/j.physletb.2012.08.021

[33] ATLAS collaboration. “Observation of a New Particle in the Search for the Standard Model Higgs Boson with the ATLAS Detector at the LHC”. Physics Letters B. 716 (1): 1-29 (2012). arXiv:1207.7214. doi:10.1016/j.physletb.2012.08.020.

[34] ATLAS collaboration; CMS collaboration (26 March 2015). “Combined Measurement of the Higgs Boson Mass in pp Collisions at âĹŽs=7 and 8 TeV with the ATLAS and CMS Experiments”. Physical Review Letters. 114 (19): 191803. arXiv:1503.07589. doi:10.1103/PhysRevLett.114.191803.

[35] LHC InternationalMasterclasses“When protons collide”. Retrieved from http://atlas.physicsmasterclasses.org/en/zpath_protoncollisions.htm

[36] CMS Collaboration, “SM Higgs Branching Ratios and Total Decay Widths (up-date in CERN Report4 2016)”.

https://twiki.cern.ch/twiki/bin/view/LHCPhysics/CERNYellowReportPageBR , last accessed on 17.12.2017.

[37] R.Grant V. “Determination of Higgs branching ratios in $H \to W^+W^- \to l\nu jj$ and $H \to ZZ \to l^+l^-jj$ channels”. Physics Department, University of Tennessee (Dated: October 31, 2012). Retrieved from http://aesop.phys.utk.edu/ph611/2012/projects/Riley.pdf

[38] LHC Higgs Cross Section Working Group, Denner, A., Heinemeyer, S. et al. “Standard model Higgs-boson branching ratios with uncertainties”. Eur. Phys. J. C (2011) 71: 1753. https://doi.org/10.1140/epjc/s10052-011-1753-8

[39] F. Maltoni, K. Paul, T. Stelzer, and S. Willenbrock, “Associated production of Higgs and single top at hadron colliders”, Phys.Rev. D64 (2001) 094023, [hep-ph/0106293].

[40] S. Biswas, E. Gabrielli, F. Margaroli, and B. Mele, “Direct constraints on the top-Higgs coupling from the 8 TeV LHC data,” Journal of High Energy Physics, vol. 07, p. 073, (2013).

[41] M. Farina, C. Grojean, F. Maltoni, E. Salvioni, and A. Thamm, “Lifting degeneracies in Higgs couplings using single top production in association with a Higgs boson,” Journal of High Energy Physics, vol. 05, p. 022, (2013).

[42] T.M. Tait and C.-P. Yuan, “Single top quark production as a window to physics beyond the standard model”, Phys. Rev. D 63 (2000) 014018 [hep-ph/0007298].

[43] F. Demartin, F. Maltoni, K. Mawatari, and M. Zaro, “Higgs production in association with a single top quark at the LHC,” European Physical Journal C, vol. 75, p. 267, (2015).

[44] CMS Collaboration, “Modelling of the single top-quark production in association with the Higgs boson at 13 TeV.” https://twiki.cern.ch/twiki/bin/viewauth/CMS/SingleTopHiggsGeneration13TeV, last accessed on 16.01.2018.

[45] CMS Collaboration, “SM Higgs production cross sections at $\sqrt{s} = 13$ TeV.” https://twiki.cern.ch/twiki/bin/view/LHCPhysics/CERNYellowReportPageAt13TeV, last accessed on 16.01.2018.

[46] S. Dawson, The effective W approximation, Nucl. Phys. B 249 (1985) 42.

[47] S. Biswas, E. Gabrielli and B. Mele, JHEP 1301 (2013) 088 [arXiv:1211.0499 [hep-ph]].

[48] F. Demartin, B. Maier, F. Maltoni, K. Mawatari, and M. Zaro, “tWH associated production at the LHC”, European Physical Journal C, vol. 77, p. 34, (2017). arXiv:1607.05862

[49] LHC Higgs Cross Section Working Group, “Handbook of LHC Higgs Cross Sections: 4.Deciphering the Nature of the Higgs Sector”, arXiv:1610.07922.

[50] J. Ellis, D. S. Hwang, K. Sakurai, and M. Takeuchi.“Disentangling Higgs-Top Couplings in Associated Production”, JHEP 1404 (2014) 004, [arXiv:1312.5736].

[51] CMS Collaboration, V. Khachatryan et al., “Precise determination of the mass of the Higgs boson and tests of compatibility of its couplings with the standard model predictions using proton collisions at 7 and 8 TeV,” arXiv:1412.8662.

[52] ATLAS and CMS Collaborations, “Measurements of the Higgs boson production and decay rates and constraints on its couplings from a combined ATLAS

and CMS analysis of the LHC pp collision data at $sqrts = 7$ and 8 TeV," (2016). CERN-EP-2016-100, ATLAS-HIGG-2015-07, CMS-HIG-15-002.

[53] File:Cern-accelerator-complex.svg. Wikimedia Commons, the free media repository. Retrieved January, 2018 from https://commons.wikimedia.org/wiki/File:Cern-accelerator-complex.svg

[54] J.L. Caron , "Layout of the LEP tunnel including future LHC infrastructures.", (Nov, 1993). A C Collection. Legacy of AC. Pictures from 1992 to 2002. Retrieved from https://cds.cern.ch/record/841542

[55] M. Vretenar, "The radio-frequency quadrupole". CERN Yellow Report CERN-2013-001, pp.207-223 DOI:10.5170/CERN-2013-001.207. arXiv:1303.6762

[56] L.Evans. P. Bryant (editors). "LHC Machine". JINST 3 S08001 (2008).

[57] CERN Photographic Service."Radio-frequency quadrupole, RFQ-1", March 1983, CERN-AC-8303511. Retrieved from https://cds.cern.ch/record/615852.

[58] CERN Photographic Service "Animation of CERN's accelerator network", 14 October 2013. DOI: 10.17181/cds.1610170 Retrieved from https://videos.cern.ch/record/1610170

[59] C.Sutton. "Particle accelerator".Encyclopedia Britannica. July 17, 2013. Retrieved from https://www.britannica.com/technology/particle-accelerator.

[60] L.Guiraud. "Installation of LHC cavity in vacuum tank.". July 27 2000. CERN-AC-0007016. Retrieved from https://cds.cern.ch/record/41567.

[61] J.L. Caron, "Magnetic field induced by the LHC dipole's superconducting coils". March 1998. AC Collection. Legacy of AC. Pictures from 1992 to 2002. LHC-PHO-1998-325. Retrieved from https://cds.cern.ch/record/841511

[62] AC Team. “Diagram of an LHC dipole magnet”. June 1999. CERN-DI-9906025 retrieved from https://cds.cern.ch/record/40524.

[63] CMS Collaboration “Public CMS Luminosity Information”. https://twiki.cern.ch/twiki/bin/view/CMSPublic/LumiPublicResults#2016_proton_proton_13_TeV_collis, last accessed 24.01.2018

[64] J.L Caron. “LHC Layout” AC Collection. Legacy of AC. Pictures from 1992 to 2002. September 1997, LHC-PHO-1997-060. Retrieved from https://cds.cern.ch/record/841573.

[65] J.A. Coarasa. “The CMS Online Cluster:Setup, Operation and Maintenance of an Evolving Cluster”. ISGC 2012, 26 February - 2 March 2012, Academia Sinica, Taipei, Taiwan.

[66] CMS Collaboration. “The CMS experiment at the CERN LHC” JINST 3 S08004 (2008).

[67] CMS Collaboration. “CMS detector drawings 2012” CMS-PHO-GEN-2012-002. Retrieved from http://cds.cern.ch/record/1433717.

[68] R. Breedon. “View through the CMS detector during the cooldown of the solenoid on February 2006. CMS Collection”, February 2006, CMS-PHO-OREACH-2005-004, Retrieved from https://cds.cern.ch/record/930094.

[69] A. Dominguez et. al. “CMS Technical Design Report for the Pixel Detector Upgrade”, CERN-LHCC-2012-016. CMS-TDR-11.

[70] CMS Collaboration. “Description and performance of track and primary-vertex reconstruction with the CMS tracker,” Journal of Instrumentation, vol. 9, no. 10, p. P10009,(2014).

[71] CMS Collaboration and M. Brice. “Images of the CMS Tracker Inner Barrel”, November 2008, CMS-PHO-TRACKER-2008-002. Retrieved from https://cds.cern.ch/record/1431467.

[72] M. Weber. “The CMS tracker”. 6th international conference on hyperons, charm and beauty hadrons Chicago, June 28-July 3 2004.

[73] CMS Collaboration. “Projected Performance of an Upgraded CMS Detector at the LHC and HL-LHC: Contribution to the Snowmass Process”. Jul 26, 2013. arXiv:1307.7135

[74] L. Veillet. “End assembly of HB with EB rails and rotation inside SX ”,January 2002. CMS-PHO-HCAL-2002-002. Retrieved from https://cds.cern.ch/record/42594.

[75] J. Puerta-Pelayo.“First DT+RPC chambers installation round in the UX5 cavern.”. January 2007, CMS-PHO-OREACH-2007-001. Retrieved from https://cds.cern.ch/record/1019185

[76] X. Cid Vidal and R. Cid Manzano. “CMS Global Muon Trigger” web site: Taking a closer look at LHC. Retrieved from https://www.lhc-closer.es/taking_a_closer_look_at_lhc/0.lhc_trigger

[77] WLCG Project Office, “Documents & Reference - Tiers - Structure,” (2014). http://wlcg.web.cern.ch/documents-reference , last accessed on 30.01.2018.

[78] CMS Collaboration. “CMSSW Application Framework”, https://twiki.cern.ch/twiki/bin/view/CMSPublic/WorkBookCMSSWFramework, last accesses 06.02.2018

[79] A. Buckleya, J. Butterworthb, S. Giesekec, et. al. “General-purpose event generators for LHC physics”. arXiv:1101.2599v1 [hep-ph] 13 Jan 2011

[80] A. Quadt. “Top Quark Physics at Hadron Colliders”. Advances in the Physics of Particles and Nuclei. Springer-Verlag Berlin Heidelberg. DOI: 10.1007/978-3-540-71060-8 (2007)

[81] DurhamHep Data Project, “The Durham HepData Project - PDF Plotter.” http://hepdata.cedar.ac.uk/pdf/pdf3.html , last accessed on 02.02.2018.

[82] F. Maltoni, G. Ridolfi, and M. Ubiali, “b-initiated processes at the LHC: a reappraisal,” Journal of High Energy Physics, vol. 07, p. 022, (2012).

[83] B. Andersson, G. Gustafson, G.Ingelman and T. Sjostrand, “Parton fragmentation and string dynamics”, Physics Reports, Vol. 97, No. 2-3, pp. 31-145, 1983.

[84] CMS Collaboration, “Event generator tunes obtained from underlying event and multiparton scattering measurements;” European Physical Journal C, vol. 76, no. 3, p. 155, (2016).

[85] J. Alwall et. al., “The automated computation of tree-level and next-to-leading order differential cross sections, and their matching to parton shower simulations,” Journal of High Energy Physics, vol. 07, p. 079, (2014).

[86] S. Frixione, P. Nason, and C. Oleari, “Matching NLO QCD computations with Parton Shower simulations: the POWHEG method,” Journal of High Energy Physics, vol. 11, p. 070, (2007).

[87] S. Agostinelli et al., “GEANT4: A Simulation toolkit,” Nuclear Instruments and Methods in Physics, vol. A506, pp. 250âĂŞ303, (2003).

[88] J.Allison et.al.,“Recent developments in Geant4”, Nuclear Instruments and Methods in Physics Research A 835 (2016) 186-225.

[89] CMS Collaboration “Full Simulation Offline Guide”, `https://twiki.cern.ch/twiki/bin/view/CMSPublic/SWGuideSimulation`, last accessed 04.02.2018

[90] A. Giammanco. “The Fast Simulation of the CMS Experiment” J. Phys.: Conf. Ser. 513 022012 (2014)

[91] A.M. Sirunyan et. al. “Particle-flow reconstruction and global event description with the CMS detector”, JINST 12 P10003 (2017) `https://doi.org/10.1088/1748-0221/12/10/P10003`.

[92] The CMS Collaboration. “ Description and performance of track and primary vertex reconstruction with the CMS tracker”. JINST 9 P10009 (2014). doi:10.1088/1748-0221/9/10/P10009

[93] P. Billoir and S. Qian, “Simultaneous pattern recognition and track fitting by the Kalman filtering method”, Nucl. Instrum. Meth. A 294 219. (1990).

[94] W. Adam, R. Fruhwirth, A. Strandlie and T. Todorov, “Reconstruction of electrons with the Gaussian sum filter in the CMS tracker at LHC”, eConf C 0303241 (2003) TULT009 [physics/0306087].

[95] K. Rose, “Deterministic Annealing for Clustering, Compression, Classification, Regression and related Optimisation Problems”, Proc. IEEE 86 (1998) 2210.

[96] R. Fruhwirth, W. Waltenberger and P. Vanlaer, “ Adaptive Vertex Fitting”, CMS Note 2007-008 (2007).

[97] CMS collaboration, “Performance of CMS muon reconstruction in pp collision events at $\sqrt{s} = 7$ TeV ”, JINST 7 P10002 2012, [arXiv:1206.4071].

[98] M. Cacciari, G. P. Salam, and G. Soyez, "The anti-k_t jet clustering algorithm," Journal of High Energy Physics, vol. 04, p. 063, (2008).

[99] B. Dorney. "Anatomy of a Jet in CMS". Quantum Diaries. June 1st, 2011. Retrieved from `https://www.quantumdiaries.org/2011/06/01/anatomy-of-a-jet-in-cms/`

[100] The CMS Collaboration."Event Displays from the high-energy collisions at 7 TeV", May 2010, CMS-PHO-EVENTS-2010-007, Retrieved from `https://cds.cern.ch/record/1429614`.

[101] The CMS collaboration. "Determination of jet energy calibration and transverse momentum resolution in CMS". JINST 6 P11002 (2011). `http://dx.doi.org/10.1088/1748-0221/6/11/P11002`

[102] The CMS Collaboration, "Introduction to Jet Energy Corrections at CMS.". `https://twiki.cern.ch/twiki/bin/view/CMS/IntroToJEC`, last accessed 10.02.2018.

[103] CMS Collaboration Collaboration. "Identification of b quark jets at the CMS Experiment in the LHC Run 2". Tech. rep. CMS-PAS-BTV-15-001. Geneva: CERN, (2016). `https://cds.cern.ch/record/2138504`.

[104] CMS Collaboration Collaboration. "Performance of missing energy reconstruction in 13 TeV pp collision data using the CMS detector". Tech. rep. CMS-PAS-JME16-004. Geneva: CERN, 2016. `https://cds.cern.ch/record/2205284`.

[105] http://cms.web.cern.ch/sites/cms.web.cern.ch/files/styles/large/public/field/image/HIG1300

[106] http://cms.web.cern.ch/sites/cms.web.cern.ch/files/styles/large/public/field/image/TOP120

[107] K. Skovpen. “Event displays highlighting the main properties of heavy flavour jets in the CMS Experiment”, Aug 2017, CMS-PHO-EVENTS-2017-006. Retrieved from `https://cds.cern.ch/record/2280025`.

[108] CMS Collaboration, “Search for the associated production of a Higgs boson with a single top quark in proton-proton collisions at $\sqrt{s} = 8$ TeV”, JHEP 06 (2016) 177,doi:10.1007/JHEP06(2016)177, arXiv:1509.08159.

[109] B. Stieger, C. Jorda Lope et al., “Search for Associated Production of a Single Top Quark and a Higgs Boson in Leptonic Channels”, CMS Analysis Note CMS AN-14-140, 2014.

[110] M. Peruzzi, C. Mueller, B. Stieger et al., “Search for ttH in multilepton final states at $\sqrt{s} = 13$ TeV”, CMS Analysis Note CMS AN-16-211, 2016.

[111] CMS Collaboration, “Search for H to bbar in association with a single top quark as a test of Higgs boson couplings at $\sqrt{s} = 13$ TeV”, CMS Physics Analysis Summary CMS-PAS-HIG-16-019, 2016.

[112] B. Maier, “SingleTopHiggProduction13TeV”, February, 2016. https://twiki.cern.ch/twiki/bin/viewauth/CMS/SingleTopHiggsGeneration13TeV.

[113] M. Peruzzi, F. Romeo, B. Stieger et al., “Search for ttH in multilepton final1 states at $\sqrt{s} = 13$ TeV”, CMS Analysis Note CMS AN-17-029, 2017.

[114] B. WG, “BtagRecommendation80XReReco”, February, 2017. https://twiki.cern.ch/twiki/bin/view/CMS/BtagRecommendation80XReReco.